Electrochemical Performance of LiNi$_{0.3}$Co$_{0.3}$Mn$_{0.3}$O$_2$-Li$_{1.3}$Al$_{0.3}$Ti$_{1.7}$(PO$_4$)$_3$ Composites Prepared by Dielectric Barrier Discharge Plasma Assisted Milling

Xing Hua Liang[1], Yu Chao Zhao[*], Di Han[1], Qing Quan Chang[1], Mei Hong Huang[1]

Guangxi Key Laboratory of Automobile Components and Vehicle Technology, Guangxi University of Science and Technology, Liuzhou 545600, China
[*]E-mail: zyc19910815@foxmail.com

The development of electric vehicles and portable electronic devices demand lighter and thinner batteries with improved specific charge and rate capabilities. In this work, we prepared LiNi$_{0.3}$Co$_{0.3}$Mn$_{0.3}$O$_2$ (NCM) using a co-precipitation route. Li$_{1.3}$Al$_{0.3}$Ti$_{1.7}$(PO$_4$)$_3$(LATP) was synthesized using a solid state reaction method. LiNi$_{0.3}$Co$_{0.3}$Mn$_{0.3}$O$_2$-Li$_{1.3}$Al$_{0.3}$Ti$_{1.7}$(PO$_4$)$_3$ (NCM-LATP) composites, with spherical agglomerates of NCM particles being homogenously dispersed in micro-sized LATP matrix, had been prepared by dielectric barrier discharge plasma assisted milling (DBDP-milling) for the first time. We analyzed surface morphologies and structures of the LATP, NCM and NCM-LATP samples by using scanning electron microscopy (SEM) and X-ray diffraction (XRD). We analyze performances of model NCM-LATP materials. The results show that the NCM-LATP composites exhibits excellent cycles tability to reach 127.4, 118.7 and 109.5 mAh g^{-1} at 0.2, 0.5 and 1C (at room temperature), respectively. The NCM-LATP composites cathode and NCM cathode had a discharge capacity of 155.9 and 136.2 mAh g^{-1} at the first cycle, and the corresponding coulombic efficiencies are 92.96% and 74.75%, at 0.05 C. Charge-discharge curves, Cyclic voltammetry and AC impedance response indicated that both NCM and LATP phases in the composite cathode were involved during the oxidation-reduction reactions and the electron transport resistance in the pure NCM cathode was much higher than that in the NCM-LATP composites cathode.

1. INTRODUCTION

The development of rechargeable batteries is considerable importance to provide the best energy storage solution in the need of the increasing energy consumption of verified devices which include portable devices and EV. For several decades, lithium-ion batteries have been focused on for

their advantages, such as high energy density, longer life, safety, environment compatibility and low cost [1-3]. The most successful active material such as layered $LiCoO_2$ is the predominant cathode material due to its high capacity and excellent cycling stability [4]. However, its practical capacity is restricted to a half of theoretical capacity and Co is an expensive and toxic element, there are significant obstacles to its wider use [5]. Therefore researchers have developed new materials by reducing the stoichiometry of cobalt using nickel and manganese, which results in cheaper and safer materials while maintaining equivalent or superior theoretical volumetric and gravimetric energy densities [6-9]. Layer structured oxide compositions (in particular $LiNi_xCo_yMn_{1-x-y}O_2$) in which lithium, nickel, cobalt and manganese ions are placed in different layers. NCM have been attracting significant interest as 4V-cathode materials for LIBs. Nickel, cobalt and manganese element in NCM play different role. Nickel is conducive to improve the material energy density. Cobalt can be layered characteristics of stable materials. Manganese to reduce material costs, improve material security and structure stability. [10-14]. In order to further improve the electrochemical performance of NCM and reduce the side effects of cathode materials and electrolytes during cycling, it found that surface modification by oxides, phosphates and fluoride, such as V_2O_5 [15], H_3PO_4 [16], $AlPO_4$ [17], Al_2O_3 [18], SiP_2O_7 [19], TiO [20], AlF_3 [21,22] and CeO_2 [23] has been investigated. Surface modification of cathode materials protect the cathode from reacting with the electrolyte at high potential. Nano scale particles were synthesized in different ways to enhance the electrochemical properties of the materials [24]. Thus, the nano cathode material can increase the contact area with the electrolyte and shorten the diffusion distance of the lithium ion, so that the electrochemical performance of the nano cathode material can be improved [25].

Herein, in this paper, the synthesis of $LiNi_{1/3}Co_{1/3}Mn_{1/3}O_2$ and $Li_{1.3}Al_{0.3}Ti_{1.7}(PO_4)_3$(LATP) via co-precipitation route and a solid state reaction method, separately. It can effectively promote the powder refinement, activation and chemical reaction effect by DBDP-milling. On this basis, the DBDP-milling method was applied in the NCM-LATP composites for lithium ion batteries. We find a new method to protect the cathode from the electrolyte reaction at high potential. The electrochemical property of NCM cathode materials achieve high-performance, which were prepared by DBDP-milling with LATP.

2. EXPERIMENT

2.1 Synthesis of $LiNi_{1/3}Co_{1/3}Mn_{1/3}O_2$ and $Li_{1.3}Al_{0.3}Ti_{1.7}(PO_4)_3$

The precursor $Ni_{1/3}Co_{1/3}Mn_{1/3}(OH)_2$ powder was prepared by a co-precipitation route. Details of a typical experiment are as follows: stoichiometric amount of $NiSO_4·6H_2O$ (purity 98%), $MnSO_4·H_2O$ (purity 98.5%), and $CoSO_4·7H_2O$ (purity 96%) were dissolved in de-ionized water and stirred to reach a concentration of 2.0 mol/L. Separately, a 4.0 mol/L NaOH (purity 96%) solution containing NH_4OH (purity 25-28% NH3), serving as a chelating agent for the coprecipitation, was fed into the reactor to carefully control the pH value. After stirring constantly for 30 min, Pour the transition metal solution into a 1 L tank reactor. The resultant mixture was then heated at 323 K until viscous. The hydroxide

precipitate was then recovered, washed with de-ionized water to remove any unreacted sulphate and sodium species, filtrated, and dried at 353 K under vacuum. It was mixed with 3 wt% excess of LiOH·H$_2$O (purity 90%) and the mix powder was sintered at 723 K for 6h followed by an annealing treatment at 1123 K for 24h under air to finally obtain NCM.

For the Li$_{1.3}$Al$_{0.3}$Ti$_{1.7}$(PO$_4$)$_3$ prepared by solid-state reaction. Details of a typical experiment are as follows: 1.3mol of lithium carbonate (Li$_2$CO$_3$, purity 96%), 1.7mol of titanium dioxide (TiO$_2$, purity 98%), 3mol of ammonium dihydrogen phosphate ((NH$_4$)$_2$HPO$_4$, purity 99%) and 0.3mol of alumina (Al$_2$O$_3$, purity 97%) were mixed into the ball mill, for 6 hours. Driping anhydrous ethanol in order to play a role in lubricationand, then calcined at 1173 K for 2 h under air to finally obtain LATP.

The NCM-LATP composites was prepared by dielectric barrier discharge plasma assisted ball milling (DBDP-milling). A plasma power supply of 15 kV, current of 1.5 A and discharge frequency of 60 kHz was applied between the inner wall of the ball mill and the central electrode rod. The ball milling process (The NCM-LATP mass ratio is 5:1, the ball to powder ratio is 40:1) is carried out in an Ar atmosphere, and finally the NCM-LATP composites material was obtained.

2.2 Material characterization

The morphologies and sizes of the obtained samples was investigated using scanning electron microscopy (SEM, ΣIGMA) at 10 kV. The composition and element distribution of cathode materials were analyze by energy dispersive X-ray spectrometry (EDS, Oxford Instruments INCA). X ray diffraction (XRD; Bruker D8 Advance) with a Cu target was used to analyze the phase purity and crystal structure of the obtained samples. The X-ray detector was scanned in a diffraction angle range of 10 to 80 ° at a speed of 2 ° min^{-1}. The Laser Particles Sizers are often employed to determine particle diameter and the particle size distribution. Particle size distributions were obtained on powders dispersed in distilled water with a Laser Particle size analyzer(GSL-101BII).

2.3 electrochemical characterization

The electrochemical performance of prepared samples were investigated using coin-type cells (CR2016). Electrode preparation of the detailed steps are as follows: the 0.8g NCM, 0.1g carbon black, 0.1g PVDF mixed evenly and fed into the appropriate amount of NMP solution. Stirring for 6 hours, the material is dispersed evenly, then mixture coated on aluminum foil and dried at 80 under vacuum for 48 hours. Disks of 16 mm diameter were punched from the foil. Special care was taken to obtain homogenous electrodes with constant thickness (~80 μm) and loading (~0.4 mAh g^{-1}). Lithium foil and a Celgard polypropylene membrane were used as the anode and the separator, respectively. The electrolyte employed was a solution of 1 M LiPF6 in a mixture of ethylene carbonate/dimethyl carbonate (EC/DMC) with 1:1 vol ratio. The assembly of coin cells was conducted in the argon-filled glove box. The electrochemical performance, scanning voltage 2.7V-4.3V and scanning rate of 0.1mV/s, were tested by the NEWARE and the CHI660E electrochemical workstation.

3. RESULTS AND DISCUSSION

3.1 Microstructure of the NCM-LATP composites

All the calcined materials were characterized by X-ray diffraction (XRD) to ensure that we obtained the expected crystalline phase. XRD patterns are presented on Fig. 1. All the diffraction peaks of NCM can be indexed to the hexagonal α-NaFeO$_2$ structure with R-3m space group. Along with traces of the characteristic peaks indicate that all materials exhibits the (006)/(102) and (018)/(110) peak separations, indicating that the samples have good hexagonal ordering and good layered characteristics [26,27]. When materials with a ratio of I(003)/I(004)>1.2, that of mixed cationic materials is relatively small, cationic homogeneous dispersed in structure [28,29].

The standard diffraction peaks of LiTi$_2$(PO$_4$)$_3$ (JCPDS card No. 35-0754) are also indicated (Fig. 1). The LATP diffraction peak corresponds to the standard card. The lattice constants calculated from the XRD data a=0.8511 nm and c=2.0788 nm are reduced, respectively. This shows that we succeeded in obtaining pure LATP, belonging to the R-3C space group.

The diffraction peaks of NCM-LATP are also displayed (Fig. 1). The sharp diffraction peaks suggest that highly crystalline, and major phase is NCM. Impurity phases were detected that were LATP. At the meanwhile, the signature of NCM and LATP no impurity phases were detected. The sharp diffraction peaks suggest that highly crystalline NCM and LATP formed.
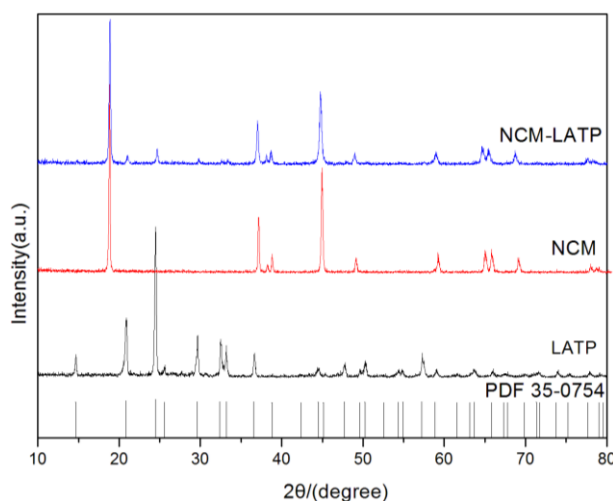
Figure 1. XRD patterns of LATP, NCM, NCM-LATP

As the SEM image clearly shown in Fig. 2. The diameter of the oxide polyhedrons(LATP) was found to be in a range of 0.15-60 μm, and it is uniform across the picture(Fig. 2a). Particle size distribution determined based on volume (insets on Fig. 2a) gives a D50 of 2.16 μm. The span value— equals to (D90-D10)/ D50, where Dx is the diameter at which x % of the population lies below—is a good indicator of the spread of the distribution [1]. SEM images of the NCM is shown on Fig. 2b. It is made of reasonably spherical agglomerates of tangled thin pellets. Particle size distribution determined based on volume (insets on Fig. 2b) gives a D50 of 6.81 μm. The value of D50 obtained for the NCM

shows the good uniformity of the size. SEM images of the NCM-LATP are shown on Fig. 2c. The mixture(NCM-LATP) looks smooth and creamy. It was found to be in a range of 0.15-3.34 μm. Particle size distribution determined based on volume (insets on Fig. 2b) gives a D50 of 1.20 μm. The value of D50 obtained for the NCM-LATP shows the good uniformity, smooth and creamy of the size. It is more tinily spherical agglomerates of tangled thin pellets than NCM.
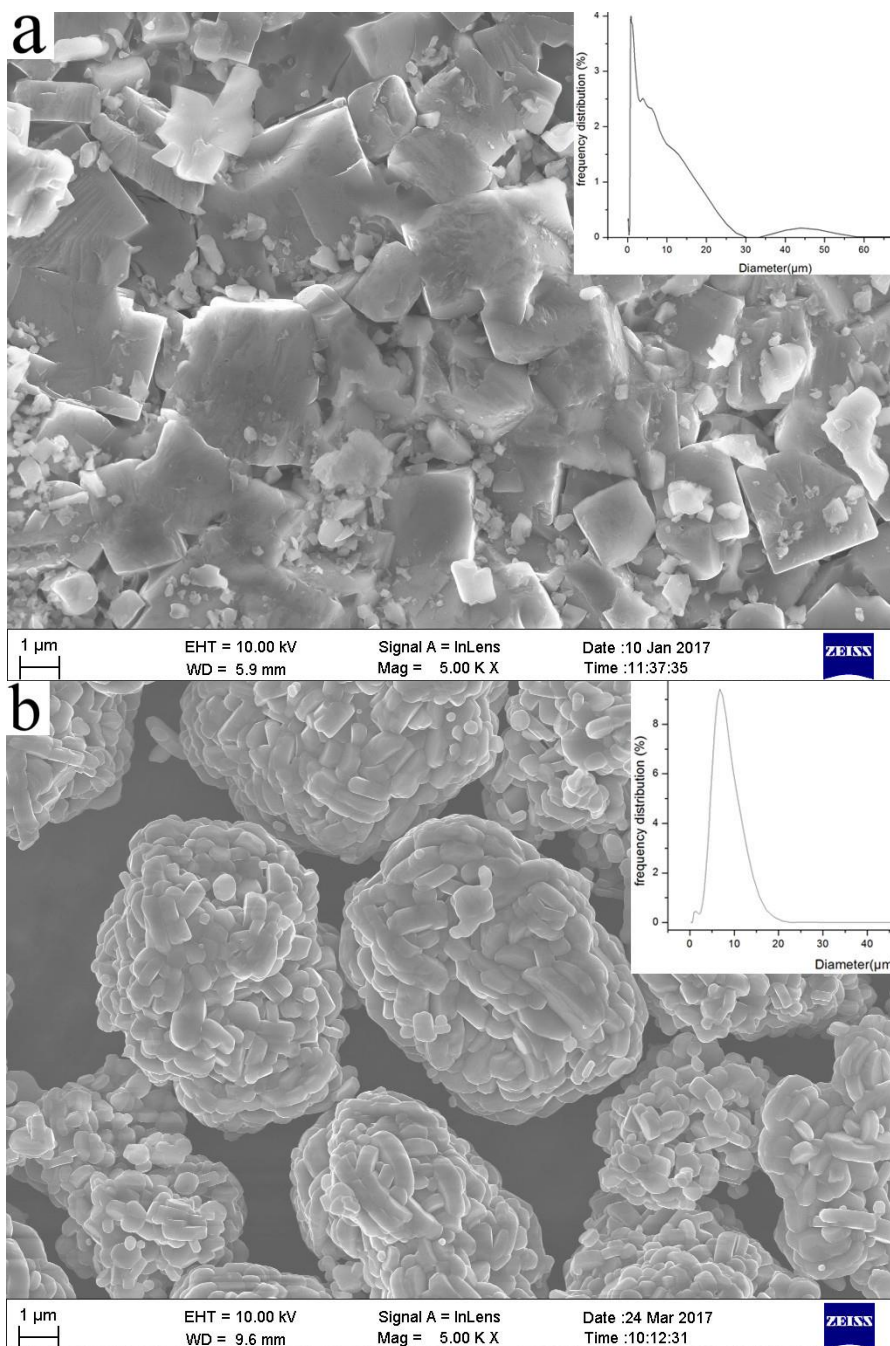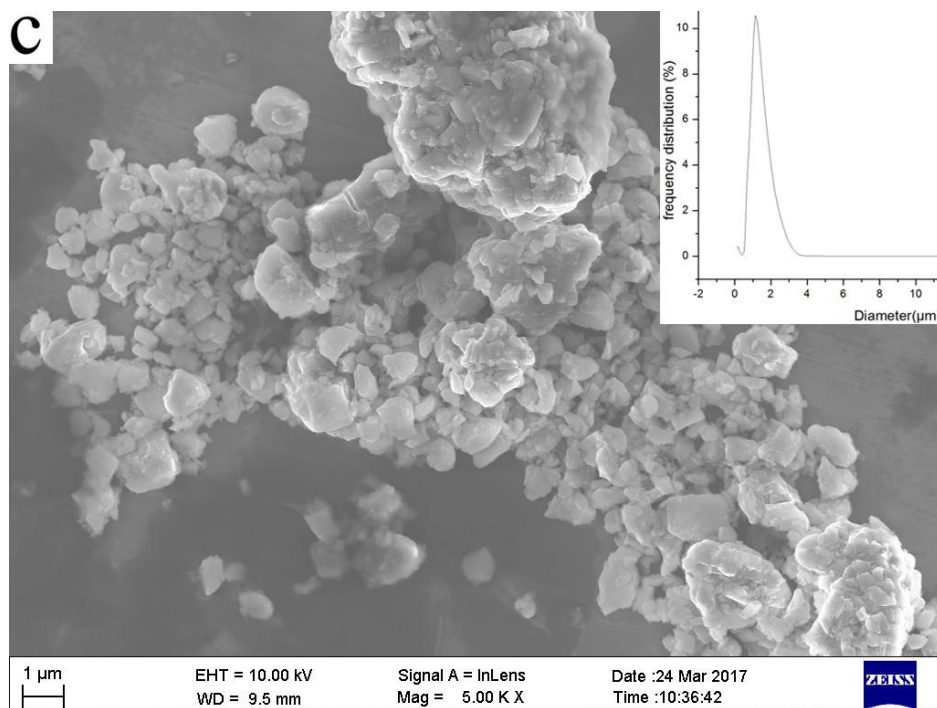
Figure 2. SEM images of LATP (a), NCM (b), NCM-LATP (c). Insets are a image of the particle size distribution.
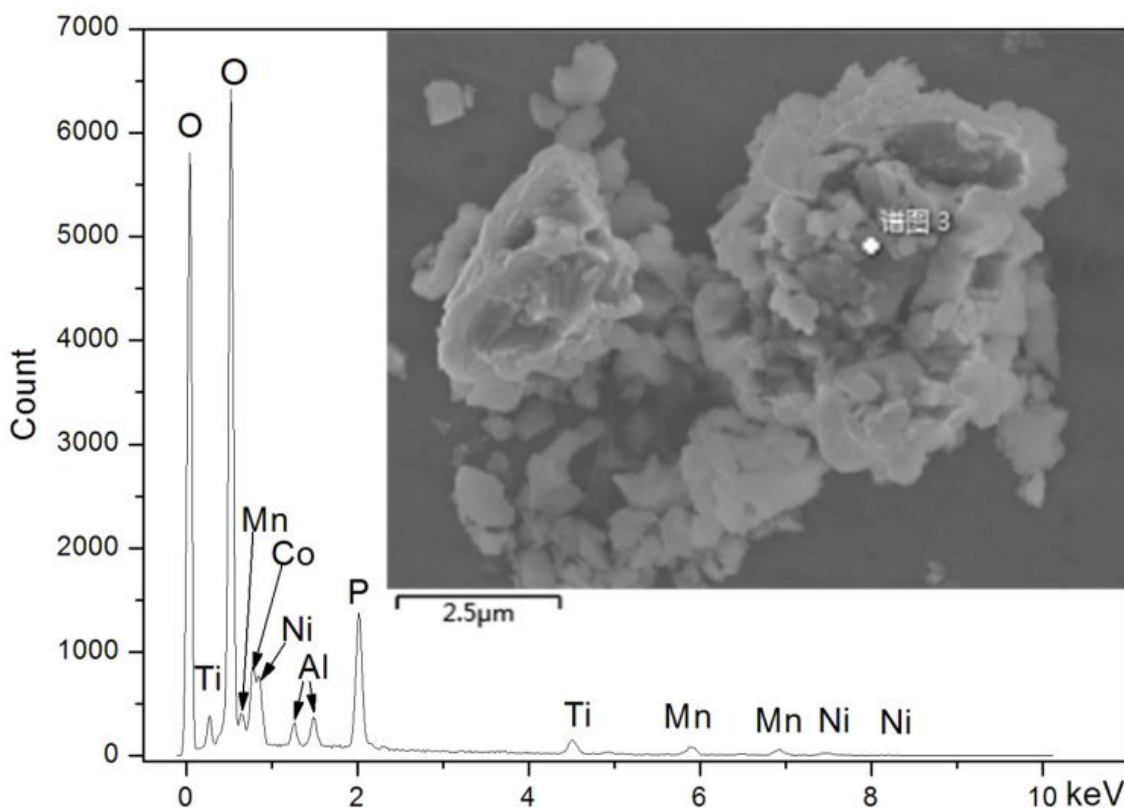

Figure 3. EDS spectra and mapping of NCM-LATP. Inset is a SEM image of the NCM-LATP.
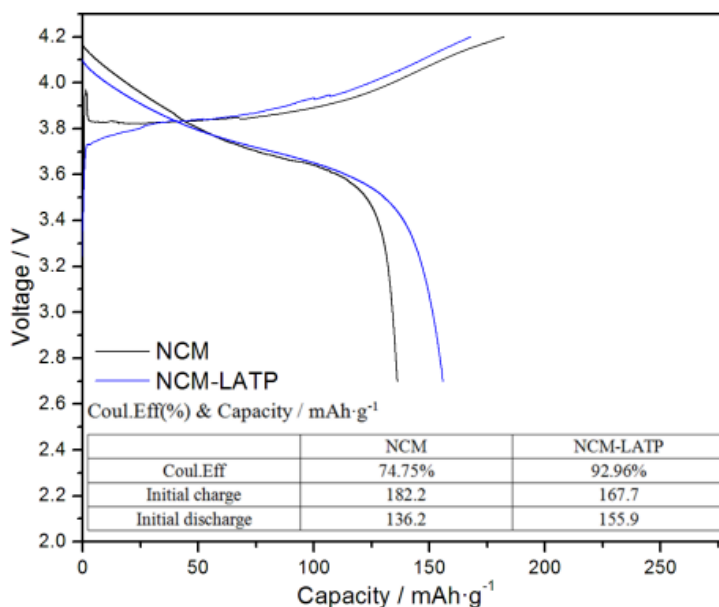
Table 2. Atomic percent composition of NCM-LATP measured by EDS

element	atomic percent
O	66.03
Al	1.82
P	9.84
Ti	3.13
Mn	4.65
Co	7.39
Ni	7.15
summation:	100.00

Fig. 4 shows the EDS spectra and mapping of NCM-LATP. It can be found the elements of Co, Mn, Ni, Ti, Al, P, and O are distributed in NCM-LATP. Table 2 shows the atomic percent of Co, Mn, Ni, Ti, Al, P, and O analyzed, the atomic ratio in the sample is equivalent to the expected values. It professed to be LATP content in NCM-LAPT.

3.2 Evaluate the electrochemical properties of the NCM and NCM-LATP

The electrochemical activity of the synthesized materials are investigated under galvanostatic conditions. The initial charge-discharge curves of the NCM and NCM-LATP are presented in fig. 4. At 0.05 C, the initial discharge capacities are 155.9 and 136.2 mAh g^{-1}for the NCM and NCM-LATP, respectively. The corresponding coulombic efficiencies are 92.96% and 74.75%, respectively. The first discharge capacity of NCM-LATP is more higher than that of NCM, and the coulombic efficiency is a much higher. The good performance of NCM-LATP benefits from DBDP-milling.

Coul.Eff(%) & Capacity / mAh·g^{-1}	NCM	NCM-LATP
Coul.Eff	74.75%	92.96%
Initial charge	182.2	167.7
Initial discharge	136.2	155.9

**Figure 4.** Initial charge/discharge performances of NCM and NCM-LATP between 2.7 and 4.3 V , current density: 0.05C

As shown in Fig. 5, CV curves of the NCM and NCM-LATP between 2.7 and 4.3 V at a scan rate of 0.1 mV s^{-1} show two distinct redox processes, which a pair of oxidation and reduction peaks centered at about 3.9 and 3.7 V, clearly observed. In the charge process, The anodic peak response near 3.9v is accompanied by the process of lithium ion extraction, the oxidation reaction of nickel ions (Ni^{2+} to Ni^{4+}) and cobalt ions (Co^{3+} to Co^{4+})[30,31]. In the discharge process, when lithium is inserted back into the structure of the electrode, the peak observed at 3.7 V corresponds to the reduction of Ni^{4+} to Ni^{2+} and Co^{4+} to Co^{3+}. Ni and Co are known to be electrochemically active elements in layered materials, and Mn with oxidation state 4$^+$ is the supporting skeleton function relatively stable. [32-35]. In Fig. 5 shows that the redox peak of NCM-LATP is sharper than NCM, and demonstrates the good reversibility of the prepared materials. After DBDP-milling, the redox peak becomes narrower, the peak width becomes narrower, and the peak current intensity increases. This indicates that the polarization of the NCM-LATP electrode has been reduced by DBDP-milling, which is beneficial to provide a good reversibility of the electrode reactions for the NCM-LATP electrode.
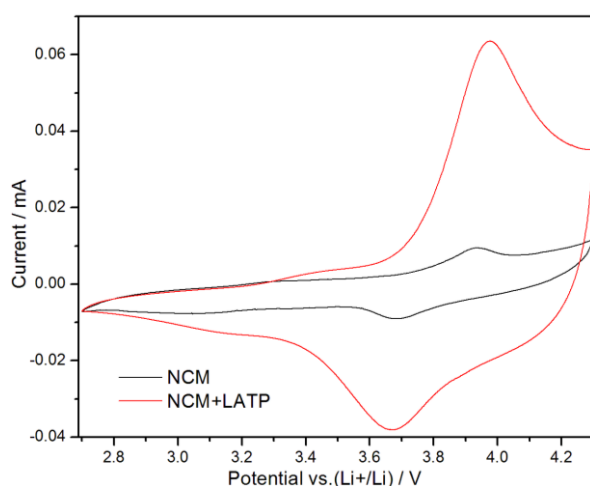
Figure 5. CV curves of the NCM and NCM-LATP between 2.7 and 4.3 V at a scan rate of 0.1 mV s^{-1}.

Fig. 6 shows the rate performance of NCM (a) and NCM-LATP (b) conducted from 0.05 C to 1 C . As increasing the charge and discharge rates, the specific capacities decrease regularly. At 0.05, 0.1, 0.2, 0.5 and 0.1, the discharge capacities of NCM-LATP are 155.1, 139.5, 127.4, 118.7 and 109.5 mAh g^{-1} respectively, but that of NCM are 136.2, 130.9, 122.2, 95.6 and 87.5 mAh g^{-1} respectively. When the current rate is increased, separation of the discharge plateaus gradually becomes blurred and the plateau voltages shift toward lower potential. NCM-LATP exhibits better rate performance than NCM, which is mainly due to the dielectric barrier discharge plasma assisted ball milling with excellent electronic conductivity, resulting in lower electrochemical impedance. The electrochemical impedance of NCM and NCM-LATP was analyzed by EIS, which was conducted after the 1st cycle (0.05 C) at room temperature.
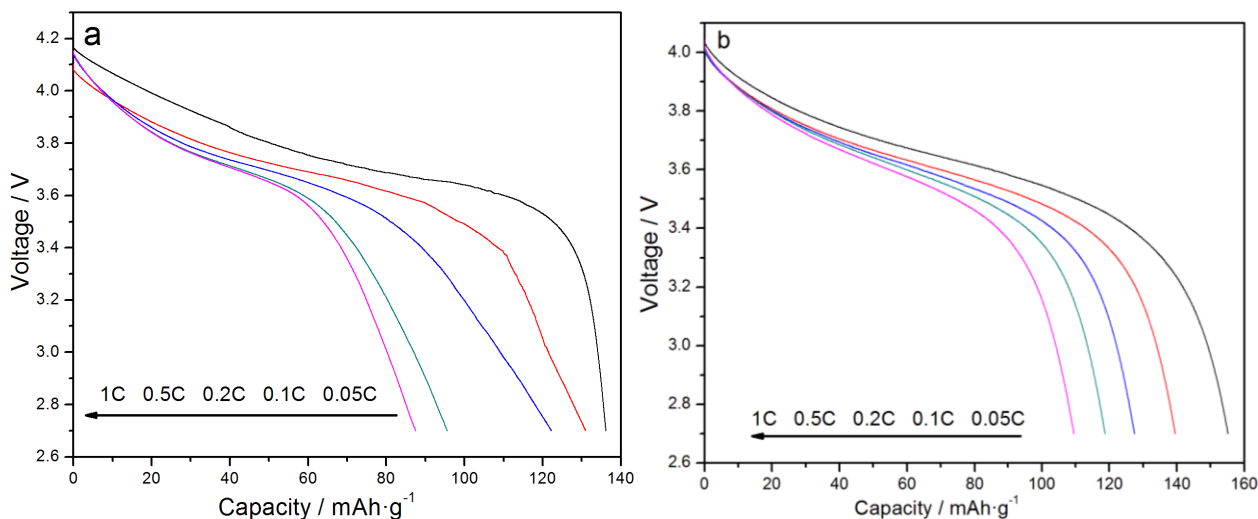
Figure 6. The rate capability of the NCM and NCM-LATP at different current rates.

The Nyquist plots are fitted and presented in Fig. 7. Fig. 7 compares the Nyquist plots of the pristine and DBDP-milling modified NCM at a charged potential of 3.6 V after the cycles. In the medium frequency region a semicircle can be found, which is related to the charge-transfer resistance of the electrode. A line at low frequency region with about 45º to the real axis is assigned to the Li^+ diffusion within the electrode. In the equivalent circuits inserted in Fig. 7c, R_e represents the uncompensated ohmic resistance, which includes the ohmic resistance in NCM or NCM-LAPT materials and the tab of cathode/anode.

Table 3. Impedance parameters evaluated from the EIS data by using equivalent circuit

Samples	$R_e(\Omega)$	$R_s(\Omega)$	$R_{ct}(\Omega)$
NCM	18.7	1037	647.9
NCM-LATP	20.6	360.5	48.99
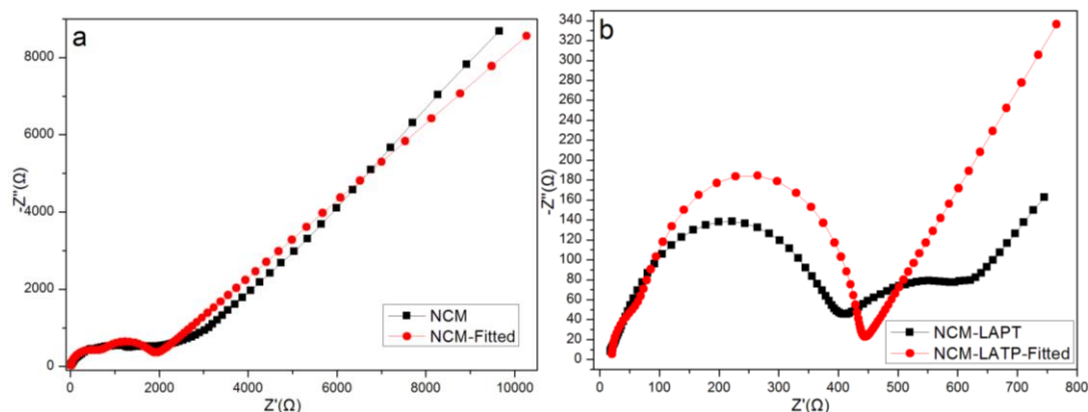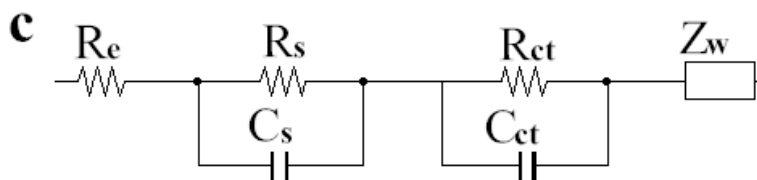
Figure 7. Fitted Nyquist plots of the NCM (a), fitted Nyquist plots of the NCM-ALTP (b) and corresponding equivalent circuits (c) of NCM and NCM-LATP

Through the analysis of the equivalent circuit, electrochemical impedance spectroscopy (EIS) data were used to discuss the resistance and ion diffusion process. The parameters R_S and C_S refer to the solid electrolyte interface impedance and ohmic impedance in the electrolyte system and capacitance of SEI, associating with the first semicircle. The parameters R_{ct} and C_{ct} correspond to the charge transfer resistance and capacitance of double-layer, associating with the second semicircle [36-39]. The parameters Zw indicates the resistance of Li$^+$ diffusion ions in the bulk material, also known as the Warburg impedance. Through the zsimdemo impedance analysis software, table 3 shows the impedance parameters of NCM and NCM-LATP fitting. Compared with the original NCM, the solid electrolyte interface impedance and charge transfer resistance decreased greatly, which indicated that plasma ball milling was beneficial to enhance the transmission of NCM-LATP and improve the rate performance of NCM-LAPT. Therefore, it is concluded that the DBDP-milling can promote the Li$^+$ inter-calation reaction at the interface between electrode and electrolytic interface. Moreover, when the size of NCM-LATP is less than nanometer, the tunneling effect can accelerate the electron migration [40]. These results corroborate the findings regarding the enhanced rate capability, cycle stability and low resistance of the DBDP-milling.

3. CONCLUSIONS

In conclusion, We synthesized NCM microspheres by co-precipitation method, and then improved the electrochemical performance of NCM by DBDP-milling. The enhanced rate capability, cycle performance and low resistance of NCM-LATP could be attributed to the dielectric barrier discharge plasma assisted ball milling surface modification, which sup-pressed the side reaction between cathode and electrolyte. At the same time, the micro morphology of NCM-LATP is even more delicate and even. This discovery opens up new opportunities for the development of high performance layered oxide cathode materials for lithium ion batteries.

References

1   C. Pierre-Etienne, P. David, C. Mikael, M. Pascal, *J. Power Sources,* 346 (2017) 13.

2   X. Jiang, S. Chu, Y. Chen, Y. Zhong, Y. Liu, Z. Shao, *J. Alloys Compd.*, 691 (2016) 206.
3   Y.C. Wang, S.X. Zhao, F. Li, C.W. Nan, *J. Alloys Compd.*, 614 (2014) 271.
4   F. Xu, H. Yan, J. Chen, M. He, Z. Zhang, C. Fan, G. Liu, *Ceram. Int.*, 43 (2017) 6494.
5   H. Li, Z. Wang, L. Chen, X. Huang, *J. Adv. Mater.*, 21 (2009) 4593.
6   E. Rossen, C.D.W. Jones, J.R. Dahn, *Solid State Ion.*, 57 (1992) 311.
7   N. Yabuuchi, T. Ohzuku, *J. Power Sources*, 119 (2003) 171.
8   T. Ohzuku, Y. Makimura, *Chem. Lett.*, 1 (2001) 642.
9   H.J. Noh, S. Youn, S.Y. Chong, Y.K. Sun, *J. Power Sources,* 233 (2013) 121.
10   J. Li, S. Xiong, Y. Liu,Z. Ju, Y. Qian, *Nano Energy,* 2 (2013) 1249.
11   C. Deng, S. Zhang, B.L. Fu, S.Y. Yang, L. Ma, *J. Alloys Compd.*, 496 (2010) 521.
12   W. Liu, M. Wang, X.L. Gao, W. Zhang, J. Chen, H. Zhou, X. Zhang, *J. Alloys Compd.*, 543 (2012) 181.
13   Z. Liu, A. Yu, J.Y. Lee, *J. Power Sources* 81 (1999) 416.
14   T. Ohzuku, Y. Makimura, *Chem. Lett.*, 1 (2001) 642.
15   X. Liu, P. He, H. Li, M. Ishida, H. Zhou, *J. Alloys Compd.*, 552 (2013) 76.
16   Y. Yao, H. Liu, G. Li, H. Peng, K. Chen, *Electrochim. Acta*, 113 (2013) 340.
17   L. Li, Y. Cao, H. Zheng, C. Feng, *J. Mater. Sci. Mater. Electron.*, 28 (2016) 1.
18   Y. Shi, M. Zhang, D. Qian, Y.S. Meng, *Electrochim. Acta,* 203 (2016)154.
19   Y.S. Lee, D. Ahn, Y.H. Cho, T.E. Hong, J. Cho, *J. Electrochem. Soc,* 158 (2010) A1354.
20   J. Li, M. Fan, X. He, R. Zhao, C. Jiange, C. Wan, *Ionics,* 12 (2006) 215.
21   S.T Myung, K.S Lee, S.Y Chong, Y.K. Sun, K. Amine, H. Yashiro, *J. Phys. Chem.* C., 114 (2014) 4710.
22   J.M. Zheng, Z.R. Zhang, X.B. Wu, Z. Zhu, Y. Yang, *J. Electrochem. Soc.*, 155 (2008) A775.
23   F. Wu, M. Wang, Y. F. Su, S. Chen, *Acta Phys. Chim. Sin.*, 25 (2009) 629.
24   C. Yang, J. Huang, L. Huang, G. Wang, *J. Power Sources,* 226 (2013) 219.
25   Y.Z. Wang, X. Shao, H.Y. Xu, M. Xie, S.X. Deng, H. Wang, J.B. Liu, H. Yan, *J. Power Sources,* 226(2013) 140.
26   J. Cho, *Chem. Mater.*, 12 (2000) 3089.
27   K.B. Kamel, N. Amdouni, A. Abdel-Ghany, K. Zaghib, A. Mauger, F. Gendron, C.M. Julien, *Ionics,* 14 (2008) 89.
28   Y. Yao, H. Liu, G. Li, H. Peng, K. Chen, *Electrochim. Acta,* 113 (2013) 340.
29   C. Yang, X. Zhang, M. Huang, J. Huang, Z. Fang, *ACS Appl. Mat. Interfaces.*, 9 (2017) 12408.
30   Y. Hu, Y. Zhou, J. Wang, Z. Shao, *Mater. Chem. Phys.*, 129 (2011) 296.
31   J.M. Zheng, J. Li, Z.R. Zhang, X.J. Guo, Y. Yang, *Solid State Ion.*, 179 (2007) 1794.
32   Z. Yang, S. Li, S.A. Xia, Y. Jiang, W.X. Zhang, *Electrochem. Solid State Lett.*, 14 (2011) A109.
33   T. Zhao, S. Chen, L. Li, X, Zhang, R. Chen, *J. Power Sources.*, 228 (2013) 206.
34   N.N. Sinha, N. Munichandraiah, *ACS Appl. Mat. Interfaces.*, 1 (2009) 1241.
35   K.M. Shaju, G.V.S. Rao, B.V.R. Chowdari, *Electrochim. Acta.*, 48 (2002) 145.
36   X.Y. Zhou, J.J. Tang, J. Yang, Y.L. Zou, S.C. Wang, *Electrochim. Acta.*, 70 (2012) 296.
37   X. Zhou, Y, Zou, J, Yang, *J. Solid State Chem.*, 198 (2013) 231.
38   N. Zhang, T.Yang, Y.Lang, K.Sun, *J. Alloys Compd.*, 509 (2011) 3783.
39   D. Aurbach, B. Markovsky, Y. Talyossef, *J. Power Sources*, 162 (2006) 780.
40   F. Wu, M. Wang, Y. Su, S. Chen, B. Xu, *J. Power Sources*,191 (2009) 628.